MODEL FOR PREDICTING 3-D BEACH CHANGES UNDER COMPOUND ACTIONS OF WAVES AND WIND

Takuya Yokota[1], Akio Kobayashi[1], Takaaki Uda[2], Masumi Serizawa[3], Yasuhito Noshi[1] and Atsunari Katsuki[4]

A model for predicting 3-D beach changes in an extensive area including beach and backshore areas was developed, taking the effects due to both waves and windblown sand into account. In the calculation of beach changes, the BG model (a model for predicting beach changes based on Bagnold's concept) was employed, and a cellular automaton method was used to calculate the backshore changes due to the effect of windblown sand. To validate the model applicability, a reproduction calculation was carried out for the beach formed at the corner of Futtsu new port. The calculation results were in good agreement with the measurement results.

Keywords: predictive model; compound actions of waves and wind; BG model; cellular automaton method

INTRODUCTION

In Japan, there are many coasts where a large amount of windblown sand is transported. In particular, on coasts facing the Pacific Ocean and formed by the deposition of a large amount of sand supplied from large rivers, the amount of windblown sand owing to the west wind in winter is significant. Therefore, on a coast where the beach is wide and is composed of fine and medium-size sand, a coastal sand dune can be formed as a result of the transport of aeolian sand. Considering that the amount of windblown sand is very large, the effect of aeolian sand cannot be ignored in the long-term prediction of topographic changes of a coastal landform. To predict these changes, the entire process of both sand transport by waves and the redistribution of sand by wind must be included in the model. We have developed several numerical models such as the contour-line-change model (Uda, 2017) and the BG model (a model for predicting 3-D beach changes based on Bagnold's concept) (Uda et al., 2018). However, in these models, the landward boundary in the calculation domain during the sand deposition is set to be the runup height of waves, although seaward sand transport associated with the scarp formation is taken into account, and the redistribution of sand deposited as windblown sand up to the landward limit was difficult to predict.

Regarding the prediction of topographic changes caused by windblown sand, Katsuki et al. (2011) predicted the formation of a barchan by a cellular automaton method, but they only reproduced the sand dune shape and did not carry out a comparative study of the real sand dune topography. Yokota et al. (2017) predicted the formation of a blowout on a sand dune by a cellular automaton method, and then the effect of fences for preventing windblown sand was investigated using the same model (Yokota et al., 2017). In these calculations, only the sand movement caused by wind was studied, and the topographic changes were not predicted, while taking both sand movement due to waves and windblown sand into account. In this study, a model for predicting not only sand transport owing to waves but also windblown sand was developed, which is applicable to a wide area between the seabed and the backshore on a coast where windblown sand prevails.

MODEL FOR PREDICTING TOPOGRAPHIC CHANGES

In this study, the beach changes due to waves occurring in the depth zone between the closure depth h_c and the berm height h_R were predicted using the BG model (Uda et al., 2018). On the other hand, topographic changes due to windblown sand were predicted in a zone landward of the berm top by a cellular automaton method, which has been used to predict the formation of a sand dune. In the model, the continuous movement of sand between the calculation domains where topographic changes due to waves and wind occur was incorporated.

In the calculation of windblown sand by a cellular automaton method, the two most important processes, saltation and avalanche, were taken into account in reference to a numerical model by Katsuki and Kikuchi (2006) for predicting the formation of a sand dune. First, two-dimensional meshes were taken on Cartesian coordinates (x, y), and the elevation at the mesh point was set as $z(x, y, t)$. We assumed that the mesh size is sufficiently large compared with the size of the sand particles.

---

[1] Department of Oceanic Architecture & Engineering, College of Science & Technology, Nihon University, 7-24-1 Narashinodai, Funabashi, Chiba 274-8501, Japan
[2] Public Works Research Center, 1-6-4 Taito, Taito, Tokyo 110-0016, Japan
[3] Coastal Engineering Laboratory Co., Ltd., 1-22-301 Wakaba, Shinjuku, Tokyo 160-0011, Japan
[4] College of Science & Technology, Nihon University, 7-24-1 Narashinodai, Funabashi, Chiba 274-8501, Japan

(a) No windblown sand $(B < b')$

(b) Windblown sand $(0 < b < 10\ m)$
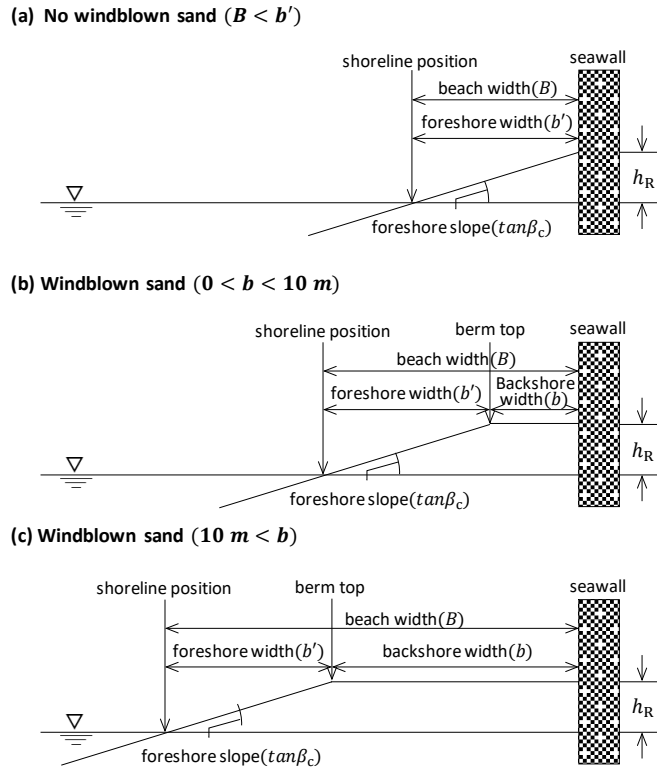
(c) Windblown sand $(10\ m < b)$

Figure 1. Classification of occurrence of windblown sand corresponding to beach width.

Saltation is a process whereby sand particles are transported by wind action, and the saltation distance L_s is defined by Eq. (1). Equation (1) is the simplest polynomial expression that can be used to evaluate the observed results of the sand flux on a sand dune including multiphase flow (Andreotti et al., 2002).

$$L_S = C_1 + C_2 z(x, y, t) - C_3 z^2(x, y, t) \qquad (1)$$

C_1, C_2, and C_3 are the coefficients used to control sand transport flux, expressed by the product of L_s defined by Eq. (1) and the moving mass of sand, and t is time. Here, we set $C_1 = 1.0$, $C_2 = 1.0$, and $C_3 = 0.01$ in this study. Eq. (1) shows that the higher the elevation where sand particles are deposited, the longer the distance that the sand particles are transported by wind, but L_s has a limit and the sand flux after the maximum value is regarded as a constant. The result of Eq. (1) was evaluated only within the domain of the increasing function, and L_s decreases at elevations higher than that where the maximum L_s occurs. Furthermore, when there is an obstacle in the field, saltation is assumed not to occur, because a vortex is formed behind an obstacle owing to the separation of the flow (Pye and Tsoar, 1990). Originally, the sand flux is given by the product of the moving mass and the saltation distance, and the sand flux can be expressed by Eq. (1) when the wind velocity is constant, assuming that the moving mass is constant. When the wind velocity changes, the coefficient of Eq. (1) can be changed in response to the wind velocity (Katsuki et al., 2011). To combine the BG model and the cellular automaton method, the calculation domains in the two methods were separated at the location of the berm, assigning the landward region of the berm as the domain of windblown sand.

The rate of windblown sand is assumed to attain an equilibrium state at a location distant from the starting point for the approach run in the downwind direction. Here, the occurrence condition of windblown sand was defined, as shown in Fig. 1, depending on the backshore width, assuming that the minimum approach run is 10 m (Horikawa et al., 1983). No windblown sand is transported when the beach width B is smaller than the foreshore width b'; the moving mass of sand (q) owing to windblown sand was given by the value multiplied by the coefficient μ shown by Eq. (2) when the backshore width b is smaller than 10 m. When b is greater than 10 m, μ is unity.

$$\mu = \frac{1}{2}\left[\cos\left(\frac{\pi}{10}b\right) + 1\right] \qquad (2)$$

GEOGRAPHICAL FEATURES OF STUDY AREA

The study area is next to Futtsu new port located 3.5 km east-northeast of Futtsu cuspate foreland, and it was constructed at the tip of the reclaimed land facing Tokyo Bay to the northwest, and a breakwater of 700 m length extends along the west side of the port (Fig. 2). In Fig. 2, the marginal lines enclosing the tidal flats A and B, which were read from a satellite image, are shown by broken lines. Offshore of the tidal flat A, a slender shallow area B extends alongshore while leaving a channel between them. In particular, area A immediately west of the fishing port has been used for gathering shellfish, and it is a very shallow tidal flat of 1.4 km length and 0.7 km width. The tidal flat A extends eastward to the front of the reclaimed land with a narrow channel extending northwestward from the fishing port, and part of the tidal flat A elongates until the breakwater of Futtsu new port. At the western corner between this breakwater and the reclaimed land, the west beach is formed owing to the sand deposition, as shown in Fig. 3, together with the formation of another beach east of the breakwater. Because eastward longshore sand transport prevails along the north shore of Futtsu cuspate foreland (Mita et al., 2014), the west beach seems to have been formed by the sand supplied by this eastward longshore sand transport. On the other hand, the Futtsu new port breakwater is sufficiently long as 700 m, and the wave height on this coast is small relative to that on the coasts facing the Pacific Ocean, because the site is located inside Tokyo Bay. Therefore, it is difficult to assume that sand was transported by waves turning around the tip of the breakwater and reached the port, resulting in the formation of the east beach. In this area, WSW wind predominantly blows, as shown in Fig. 4, so the sand deposited on the east beach is assumed to be supplied directly from the west beach as windblown sand.
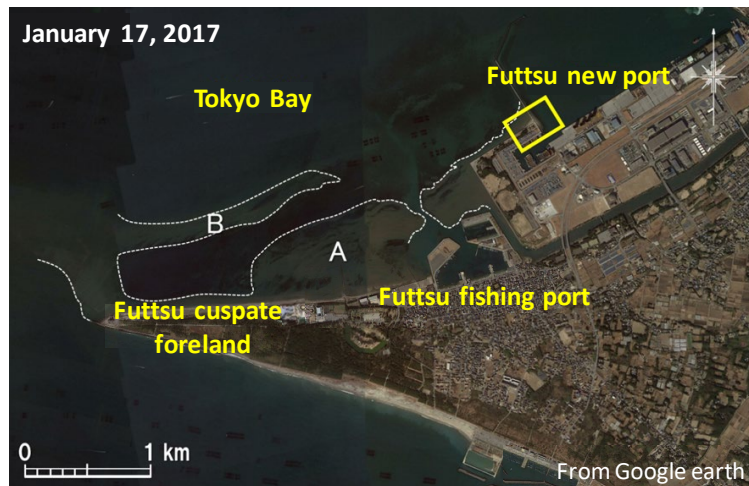

Figure 2. Location of Futtsu new port.

Figure 3. Satellite image of west and east beaches formed at corner between port breakwater and seawall.
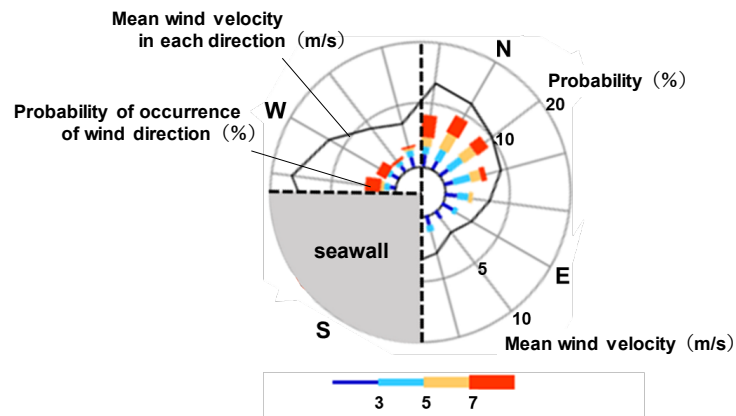
Figure 4. Wind rose at Futtsu new port (NEDO).

Figure 5. West beach formed at corner between port breakwater and reclaimed land.

Figure 6. Overall view of west beach.

FIELD OBSERVATION OF WEST AND EAST BEACHES

On July 16, 2017, field observation was carried out on the west and east beaches, as shown in Fig. 3, as well as a beach survey using an RTK-GPS on September 23, 2017. First, Fig. 5 shows the west beach formed at the corner between the port breakwater and the seawall of the reclaimed land. A sandy beach was formed while burying the basement rocks in front of the seawall. The height of this beach seemed to be the same as or slightly larger than the crown of the port breakwater, and the upper part was covered with coastal vegetation. Figure 6 shows an overview of the west beach taken from on top of the port breakwater. A stable beach extended west of the port breakwater with a wide foreshore. The east end of the west beach is shown in Fig. 7. The height of the west beach covered with *Carex kobomugi* was larger than the crown height of the port breakwater, and sand was partly deposited on the crown of the breakwater. From this fact, it was realized that sand was transported from the west beach to the east

Figure 7. Sand deposition along east end of west beach and over port breakwater.

Figure 8. Sand deposition on slope along eastern edge of port breakwater.

Figure 9. Overview of east beach.

beach over the crown of the port breakwater by the west wind, even though the beach surface was covered with coastal vegetation. Figure 8 shows the east edge of the port breakwater. Sand covered the top of the concrete blocks placed along the eastern edge of the port breakwater, implying that the sand was transported eastward by wind over the reclaimed land and deposited on top of the concrete blocks. The fact that the top of the slope over the concrete blocks, which was formed by the sand deposition, had the same height as the crown of the port breakwater is evidence that sand was transported from over the walkway inside the fence by wind. Finally, Fig. 9 shows the east beach with a semicircular shape; this beach was considerably inland of the offshore part of the port breakwater.

The beach topography was measured along the transects shown in Fig. 10. On the west beach, 11 transects were set in the direction normal to the seawall at an interval of 6 m, whereas on the east beach,19 transects were set in the direction normal to the port breakwater. The interval of the transects on the east

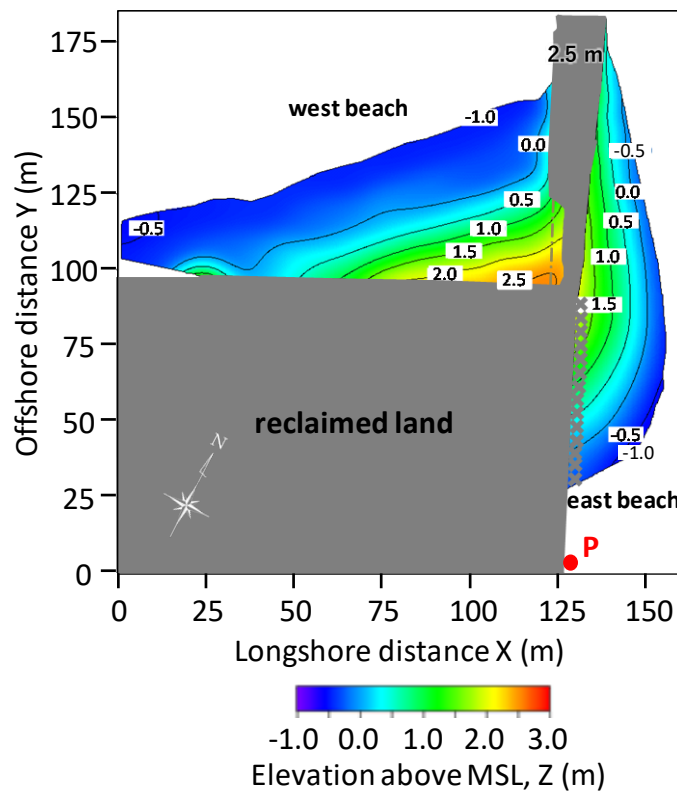**Figure 10. Alignment of transects on west and east beaches.**

Figure 11. Topographies of west and east beaches.

beach was 10 m between transect No. 1 and No. 10, whereas the interval was set to 6 m south of transect No. 11.

Figure 11 shows the topographies of the west and east beaches. The elevation of the west beach is higher than that of the east beach, and the elevation of the beach where it met the port breakwater was 2.5 m above mean sea level (MSL). Sand was deposited to partly cover the crown of the breakwater from the west side, whereas the elevation of the east beach was 1.5 m, 1.0 m lower than that of the west beach. In addition, the elevation of point P south of the east beach was −2.0 m, implying that the water depth surrounding the east beach is at least 2.0 m.

The west beach was formed owing to the blockage of eastward longshore sand transport by the port breakwater, and the longitudinal profile along each transect was formed owing to the deposition of sand over time. By using the ergodic rationale for beach changes, the longshore change in the beach
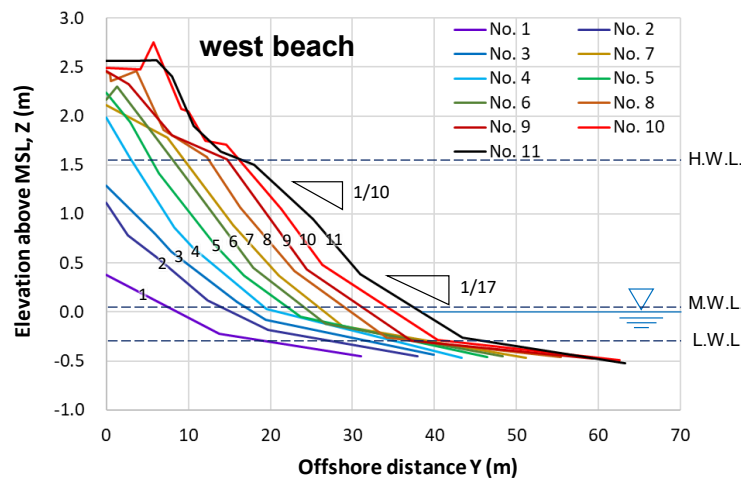
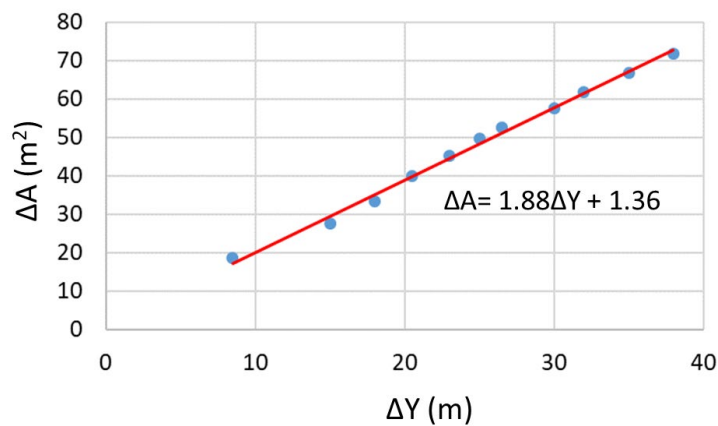**Figure 12. Superimposed profiles on west beach.**

Figure 13. Correlation between cross-sectional area of the beach and change in shoreline position.

profile can be used to explain the temporal changes in the profile by substituting time for space (Uda, 2017), i.e., the change in profile along transect No. 1 over time can be explained by the longshore change in profiles between transects No. 1 and No. 11. In other words, the shape of the initial profile is maintained along transect No. 1, whereas the profile after a sufficiently long time has passed is assumed to be maintained along transect No. 11. Under this condition, the superimposed profiles between transects No. 1 and No. 11 indicate the temporal change in the profile when sand was gradually deposited. Thus, profiles were superimposed with reference to the seawall line, as shown in Fig. 12. The beach slope gradually increased and a beach profile with a constant foreshore slope developed near transect No. 4. The profile showed a change in slope near the elevations $z = 0.5$ and 1.5 m, and the slope between $z = 0.1$ and 0.5 m is 1/17, and that between $z = 0.5$ and 1.5 m is 1/10. The profile changes as if the longitudinal profile moves in parallel in the cross-shore direction. Furthermore, a constant water depth of -0.5 m extends in the offshore area, and the area with elevation greater than $z = 1.5$ m corresponds to the area covered with coastal vegetation.

Next, in Fig. 12, the change in the foreshore area (ΔA) in the elevation range between $z = -0.5$ and 1.5 m and the change in shoreline position (ΔY) were calculated with reference to the profile along transect No. 1. Then, the characteristic height of beach changes was determined as the regression coefficient between the cross-sectional area of the beach and the change in shoreline position, as shown in Fig. 13. The characteristic height of beach changes was determined to be 1.88 m with $R^2 = 1.0$.

Similarly, the results of the analysis of the profile changes on the east beach are shown in Figs. 14 and 15. Figure 14 shows that there is a change in slope at $z = 1.2$ m and a constant slope of 1/10 between this point and the shoreline position. However, a slope of 1/13, gentler than the foreshore slope, was formed in the area with a height larger than $z = 1.2$ m. The foreshore slope gradually decreased between transect No. 11 and No. 19.
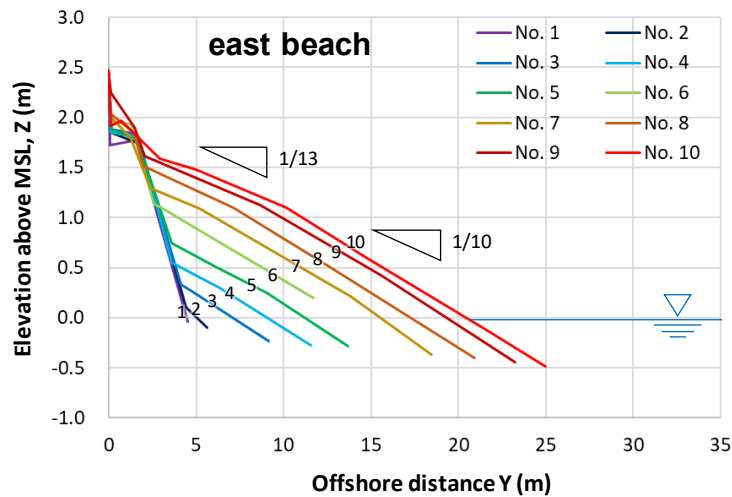
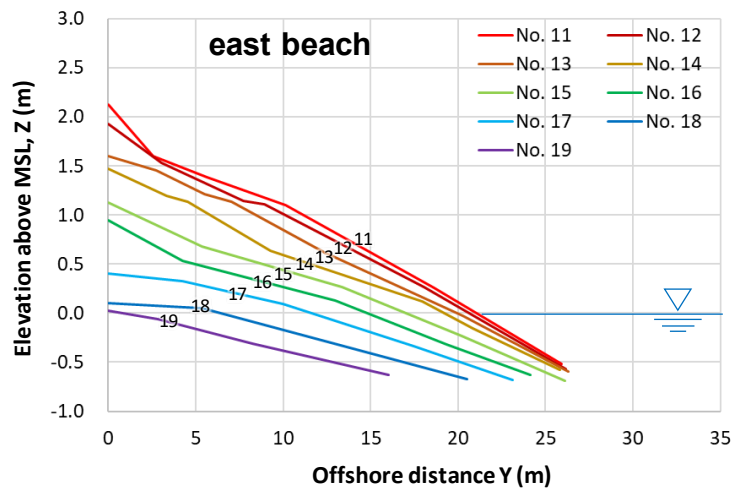**Figure 14. Superimposed profiles on east beach (transects No. 1–No. 10).**

Figure 15. Superimposed profiles on east beach (transects No. 11–No. 19).

LONG-TERM FORMATION OF WEST AND EAST BEACHES

Time-dependent changes in the west and east beaches between 2000 and 2018 are shown in Fig. 16. The west beach with a triangular shape has gradually developed at the corner between the port breakwater and the reclaimed land since 2000, and with this, the east beach which has an elongated, asymmetric shape along the port breakwater, has also developed. Because both beaches neighbor each other, the direct transport of windblown sand across the port breakwater is assumed to be the major factor in forming the east beach. The change in the areas of the west and east beaches calculated from these aerial photographs is shown in Fig. 17. The rate of increase in the foreshore area of the west beach was 106.4 m^2/yr between 2000 and 2008, and it decreased to 22.4 m^2/yr after 2008. In contrast, the rate of increase in the foreshore area of the east beach increased from 49.4 m^2/yr between 2000 and 2008 to 71.3 m^2/yr after 2008. This is because after the west beach had sufficiently developed, the transport of windblown sand from the west beach to the east beach was accelerated. There is some discrepancy in the rate of increase in the foreshore areas of the west and east beaches. This is because although shallow sea extends offshore of the west beach, the water depth offshore of the east beach is large, so the volume of sand deposited in the subsurface area becomes large. Furthermore, part of the windblown sand from the west beach was deposited in the gaps of the concrete blocks installed along the port breakwater, as shown in Fig. 8, which is another cause of the loss of sand.

By multiplying the annual changes in foreshore area obtained by comparing the aerial photographs by the characteristic height of beach changes of 1.88 m, the volume changes were calculated. In Fig. 17, the rate of increase in the foreshore area decreased from 106.4 m^2/yr before 2008 to 22.4 m^2/yr after 2008. Considering that this difference was caused by the sand transport from the west beach to the east beach,

we multiplied the difference in the reduction rate by 1.88 m, resulting in the sand supply of 158 m³/yr from the west beach to the east beach since 2008.
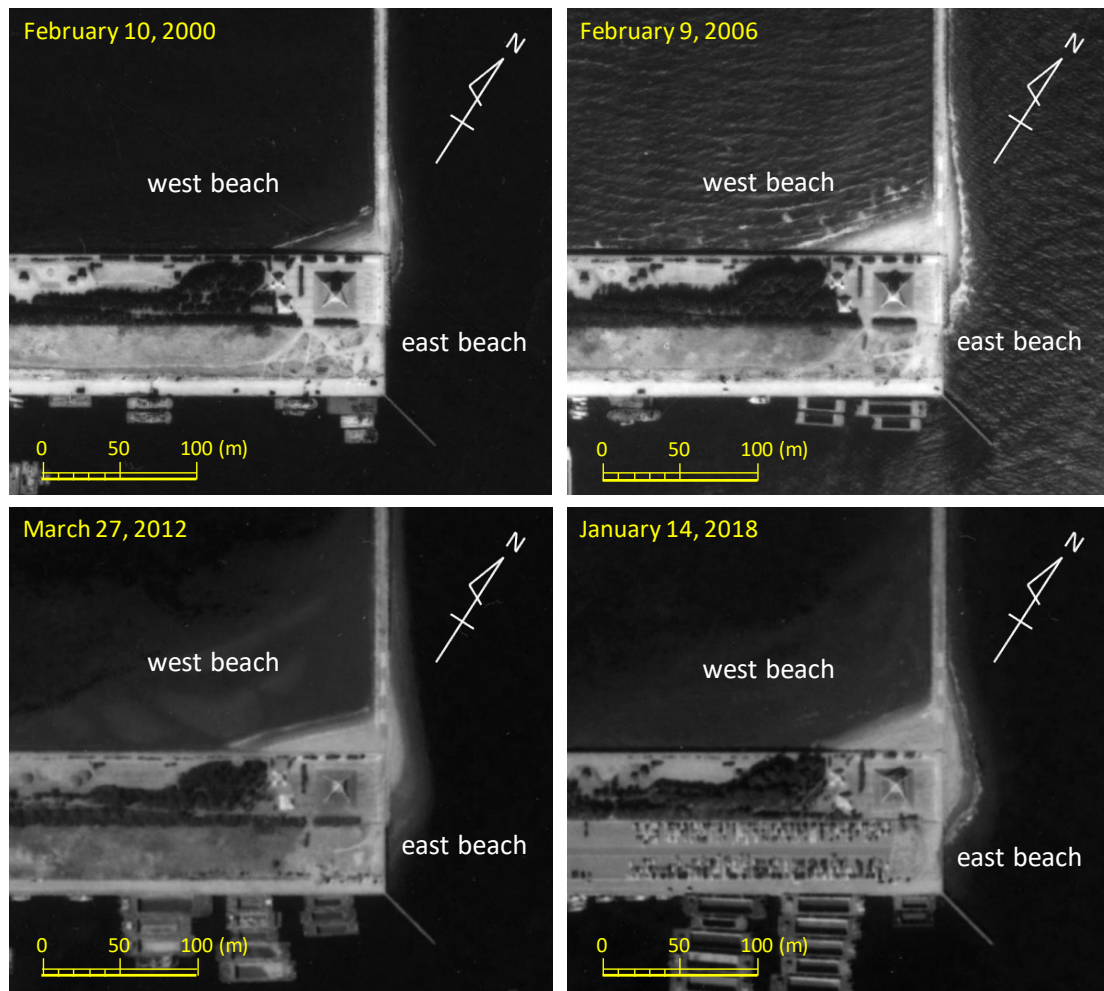

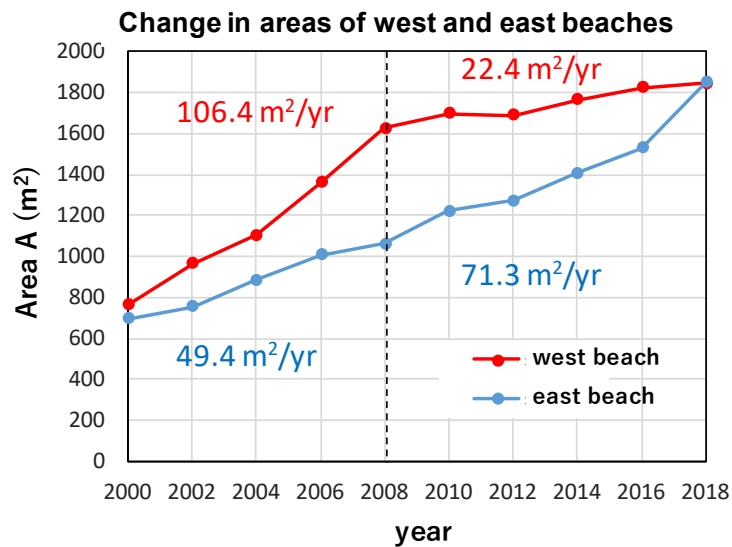**Figure 16. Beach changes at corner between port breakwater and reclaimed land.**

Figure 17. Change in foreshore areas of west and east beaches.

CALCULATION OF CROSS-SHORE SAND MOVEMENT

To verify the applicability of the present model to the prediction of sand movement owing to waves and windblown sand, the sand movement in the 2-D crosssection was considered in which wind blew in the same direction as that in the propagation of waves (-*Y* direction). Table 1 shows the calculation conditions. The depth of closure h_c and the berm height h_R were assumed to be 5 and 2 m, respectively, with an equilibrium slope of 1/20. In the initial topography, the seabed slope was assumed to be 1/20, and a flat plane beach with an elevation of 2 m above MSL was assumed landward of the berm top. Solid walls were set along the boundaries. The moving mass of sand transported by wind was assumed to be 4.0×10^{-5} m^3/m^2/step and the incident wave height was assumed to be 1.0 m.

Figure 18 shows the initial topography and the results of the calculation. The calculation results show that the windblown sand transported landward from the berm top was deposited in front of the seawall, while forming an approximately 1/5.5 slope, whereas on the beach, the shoreline receded while maintaining an equilibrium slope. Since the sand budget is satisfied, the cross section retreated in parallel in response to the volume of sand transported by wind, and the volume of sand that accumulated in front of the seawall increased.

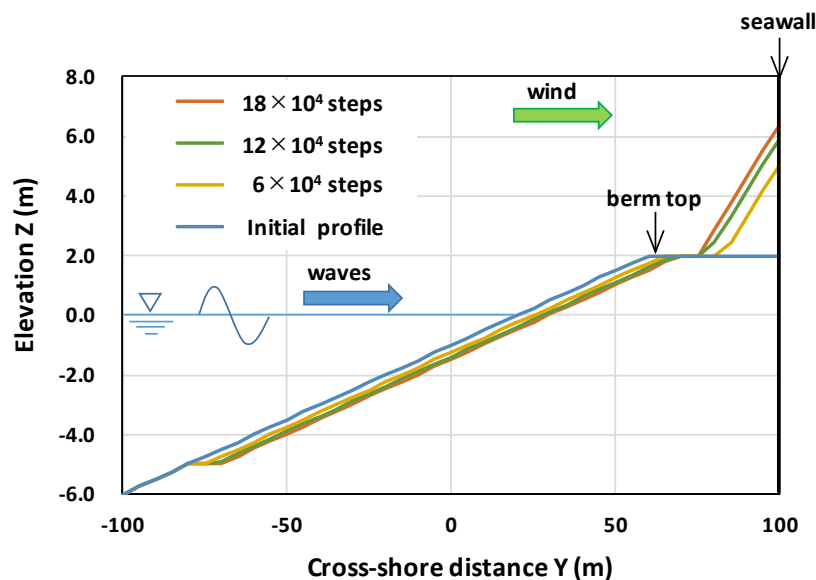| Table 1. Calculation conditions (2-D calculation).		
Equilibrium slope		1/20
Incident wave conditions	Incident wave height (m)	1.0
	Wave direction α (deg)	0.0
	Tide condition MSL (m)	0.0
Depth range of beach changes	Depth of closure h_c (m)	5.0
	Berm height h_R (m)	2.0
Coefficient of longshore sand transport	Coefficient of longshore sand transport	0.2
	Ratio of cross-shore sand transport relative to longshore sand transport	0.2
Depth distribution of sand transport		quadratic equation of depth (Uda and Kawano, 1995)
Wind direction α_w (deg)		0.0
Rate of windblown sand (m^3/m^2/step)		4.0×10^{-5}
Coefficients of equation(1)	C_1	1.0
	C_2	1.0
	C_3	0.01
Critical slope for falling sand	land area, sea area	1/2
Calculation domain	Longshore direction x (m)	500
	Cross-shore direction y (m)	200
Calculation meshes	$\triangle x$ (m)	10
	$\triangle y$ (m)	5
Time step $\triangle t$ (hr)		1
Calculation steps of year (steps)		18×10^4

Figure 18. Results of 2-D calculation.

REPRODUCTION CALCULATION OF WEST AND EAST BEACHES

The formation of the west and east beaches was reproduced using the model. Table 2 shows the calculation conditions. Wave conditions were determined on the basis of the observation data at NOWPHAS Dainikaiho wave observatory. The wind direction necessary for the calculation of windblown sand referred to the predicted one by NEDO, and the wind was assumed to blow at an angle of 70° counterclockwise relative to the seawall. The equilibrium slope, h_R, and h_c were assumed to be 1/10, 1.5 m, and 4.5 m, respectively, on the basis of the topographic survey data. The rate of the moving mass of sand was assumed to be 2.0×10^{-5} m^3/m/step, and the coefficients C_1, C_2, and C_3 in Eq. (1) were 1.0, 1.0, and 0.01, respectively, in reference to the numerical simulation of the formation of a sand dune by Katsuki et al. (2011).

Figure 19 shows the initial topography for the 3-D calculation. The crown height of the port breakwater and the walkway on the reclaimed land was 2.5 m, and the seabed depth offshore of the west

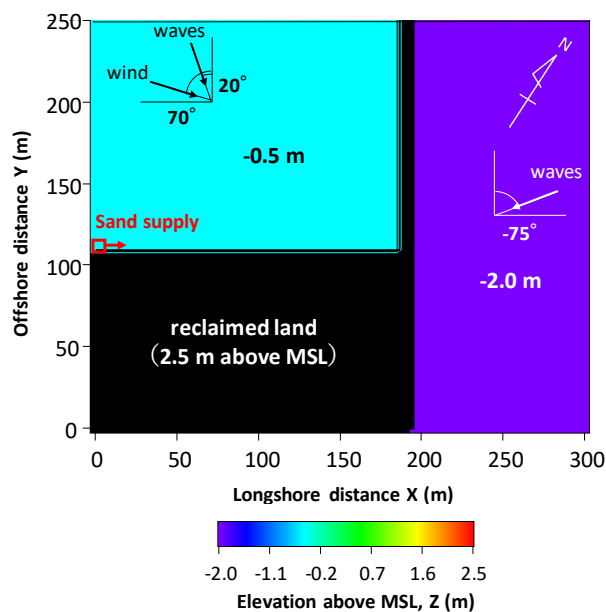| Table 2. Calculation conditions (3-D calculation).			
Equilibrium slope			1/10
Incident wave conditions	Incident wave height (m)		0.33
	Wave direction α (deg)	west of breakwater	20
		east of breakwater	-75
	Tide condition MSL (m)		0.0
Depth range of beach changes	Depth of closure h_c (m)		4.5
	Berm height h_R (m)		1.5
Coefficient of longshore sand transport	Coefficient of longshore sand transport		0.2
	Ratio of cross-shore sand transport relative to longshore sand transport		0.2
Depth distribution of sand transport			quadratic equation of depth (Uda and Kawano, 1995)
Wind direction α_w (deg)			70
Rate of windblown sand (m^3/m^2/step)			2.0×10^{-5}
Coefficients of equation(1)	C_1		1.0
	C_2		1.0
	C_3		0.01
Critical slope for falling sand	land area, sea area	west of breakwater	1/2
		east of breakwater	1/10
Calculation domain	Longshore direction x (m)		300
	Cross-shore direction y (m)		250
Calculation meshes	$\triangle x$ (m)		5
	$\triangle y$ (m)		5
Time step $\triangle t$ (hr)			1
Calculation steps of year (steps)			8760

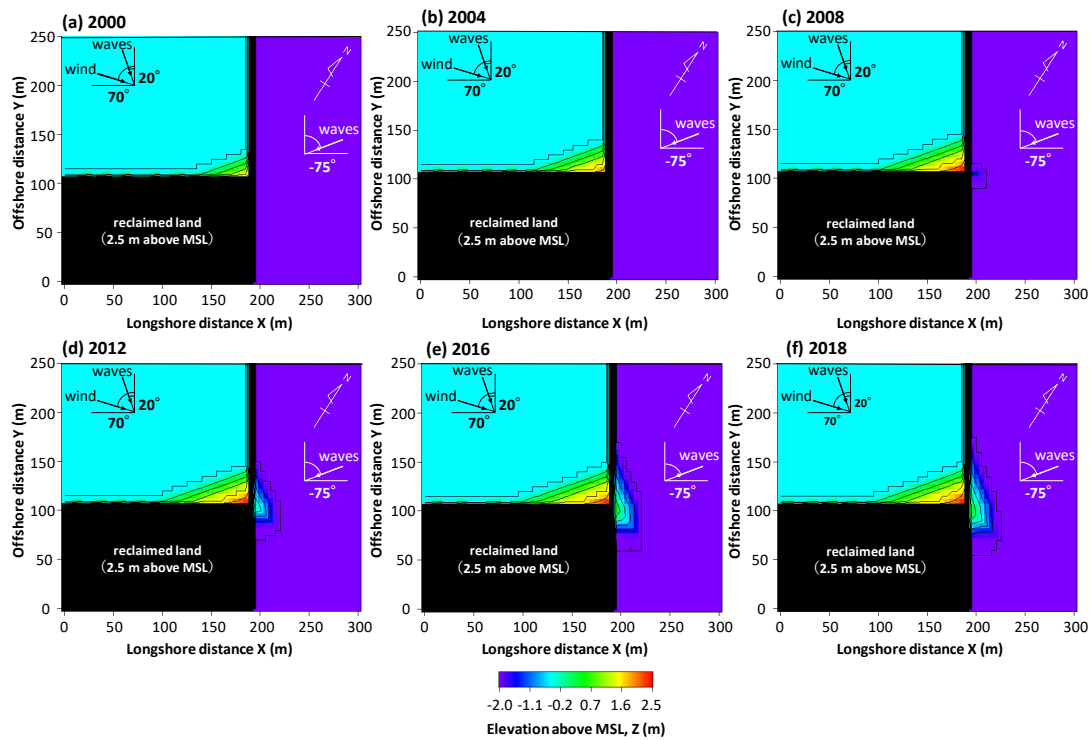**Figure 19. Initial topography for 3-D calculation.**
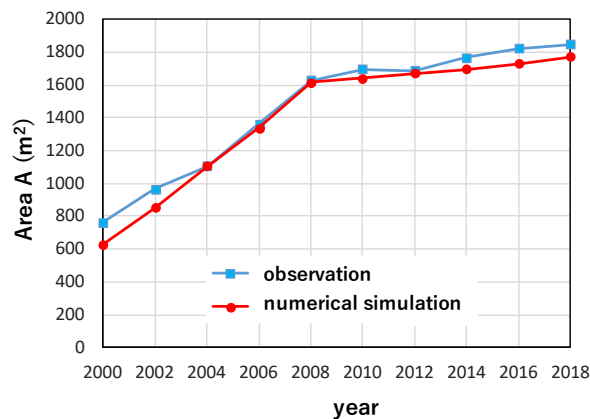
Figure 20. Results of 3-D calculation.

Figure 21. Comparison of measured and calculated changes in area of west beach.

beach was given as 0.5 m from the observation results, and a solid bed with a constant depth of 0.5 m was assumed. Although the exact water depth offshore of the east beach was unknown, a constant water depth of −2.0 m (solid bed) was assumed, because the maximum water depth measured near the east beach was 2.0 m at point P. Sand was supplied from the west end of the calculation domain at every step. The results of the calculation between 2000 and 2018 are shown in Fig. 20. The west beach has gradually formed since 2000, and windblown sand was transported over the port breakwater over time and deposited inside the port after 2008. At the corner of the port breakwater and the seawall, windblown sand has been deposited, and the ground elevation has increased. This is in good agreement with the conditions measured in the field observation. Figure 21 shows the change in the beach areas of the west beach measured from the aerial photographs and calculated in the reproduction calculation. In the calculation, the development of the west beach started in 2000, and then windblown sand was transported inside the port from the west beach over the port breakwater after 2008, resulting in the decrease in the rate of the development of the west beach. These results are in good agreement with the changes observed from the aerial photographs. Furthermore, the rate of increase in the volume of the east beach calculated since 2008 was 164.4 m^3/yr. It was in good agreement with the value of 158 m^3/yr estimated from the field data.

CONCLUSIONS

A model for predicting topographic changes owing to not only waves but also windblown sand was developed by combining the BG model and a cellular automaton method. To verify the effectiveness of the model, field investigation and the analysis of aerial photographs were carried out, taking the beaches formed at the corner between the breakwater of Futtsu new port and reclaimed land as an example. With these field data, the model was reproduced. It was found that windblown sand was transported from the west beach to the east beach over the port breakwater. The results of the numerical simulation were in good agreement with the measurement results. In the present model, the topographic changes caused by not only waves but also windblown sand can be predicted simultaneously.

REFERENCES

Andreotti, B., Claudin, P., and Douady, S. 2002. Selection of dune shapes and velocities Part 1: Dynamics of sand, wind and barchans, Eur. Phys. J., B 28, pp. 321-339.

Horikawa, K., Hotta, S., Kubota, S., and Katori, K. 1983. Field observation of windblown sand by trench trap, J. Jpn. Coastal Eng., Vol. 30, pp. 406-410.

Katsuki, A. and Kikuchi, M. 2006. Simulation of barchan dynamics with interdune sand stream, RIMS Kokyuroku, 1472, pp. 67-70. (in Japanese)

Katsuki, A., Nishimori, H., Kikuchi, M., Endo, N., and Taniguchi, K. 2011. Cellular model for sand dunes with saltation, avalanche and strong erosion: collisional simulation of barchans, Earth Surface Processes and Landforms, Vol. 36, pp. 372-382.

Mita, K., Kobayashi, A., Uda, T., and Noshi, Y. 2014. Beach changes along northern coast of Futtsu cuspate foreland and effect of 2011 Great Tsunami, J. JSCE, B3 (Civil Engineering in the Ocean), Vol. 70, No. 2, pp. I_600-I_605. (in Japanese)

NEDO: http://app8.infoc.nedo.go.jp/nedo/

Pye, K. and Tsoar, H. 1990. Aeolian Sand and Sand Dunes, Unwin Hyman, London, pp. 42-43.

Uda, T. 2017. Japan's Beach Erosion - Reality and Future Measures, 2nd ed., Singapore, World Scientific, 530 pp.

Uda, T., Serizawa, M., and Miyahara, S. 2018. Morphodynamic model for predicting beach changes based on Bagnold's concept and its applications, INTEC, London, UK, p. 188. https://www.intechopen.com/books/morphodynamic-model-for-predicting-beach-changes-based-on-bagnold-s-concept-and-its-applications

Yokota, T., Kobayashi, A., Uda, T., Serizawa, M., Katsuki, A., and Noshi, Y. 2018. Model for predicting formation of blowout on coastal sand dune using cellular automaton method, Proc. 36th Conf. on Coastal Eng., Baltimore, Maryland, papers.40, pp. 1-12. https://journals.tdl.org/icce/index.php/icce/article/view/8413/7221

Yokota, T., Kobayashi, A., Uda, T., Serizawa, M., Katsuki, A., and Noshi, Y. 2017. Model for predicting formation of blowout on coastal sand dune using cellular automaton method, Proc. 9th Int. Conf. on Asian and Pacific Coasts (APAC2017), pp. 572-583.

Yokota, T., Kobayashi, A., Uda, T., Katsuki A., and Noshi, Y. 2018, Topographic changes around sand fence for predicting windblown sand and its prediction using cellular automaton method, J. JSCE, B3 (Civil Engineering in the Ocean), Vol. 74, No. 2, pp. I_749-I_754.